Article publicat / *Published paper*:

Hamdi, E. [et al.]. Robust stability of stochastic systems with varying delays: application to RLC circuit with intermittent closed-loop. "Applied mathematics and computation", 15 Desembre 2021, vol. 411, art. 126541. DOI: 10.1016/j.amc.2021.126541

Robust stability of stochastic systems with varying delays: application to RLC circuit with intermittent closed-loop ☆

Issam El Hamdi[a], Alessandro N. Vargas[b,1,*], Hassane Bouzahir[a], Ricardo C. L. F. Oliveira[c], Leonardo Acho[d]

[a] *LISTI, ENSA, Ibn Zohr University, PO Box 1136, Agadir, Morocco.*
[b] *Universidade Tecnológica Federal do Paraná, UTFPR, Av. Alberto Carazzai 1640, 86300-000 Cornelio Procópio-PR, Brazil.*
[c] *Universidade Estadual de Campinas, UNICAMP, FEEC, Av. Albert Einstein 400, 13083-852 Campinas-SP, Brazil.*
[d] *Universitat Politècnica de Catalunya Barcelona Tech, Department of Mathematics, 08222 Terrassa, Barcelona, Spain.*

Abstract

This paper characterizes the robust second-moment stability of stochastic linear systems subject to varying delays. The delays assume a particular form suitable to represent packet loss in networked control systems, under the zero-order hold feedback. The proposed robust stability condition requires checking the spectral radius of an appropriate matrix that that depends on uncertain parameters belonging to a polytope. Due to this polytope's dependence, checking the spectral radius is difficult from the numerical viewpoint. As an attempt to solve the problem, we convert the polytope-based condition into a randomized approach. Namely, we present probability bounds that help us certificate the robust second-moment stability under high probability. A real-time electronic application illustrates the potential benefits of our approach.

Keywords: Stochastic systems; Markov jump linear systems; Stochastic stability; Robust stability; Packet dropout; RLC circuits.

---

1. Introduction

The Markov chain has been used intensively in modeling packet loss over networks [16, 25, 46, 47, 48], along with other applications such as in DC motors [34], electronic converter [1], vehicle-to-vehicle communication [26], platoon of vehicles [43], and internet of things [8]. Markov chain also plays a key role in the control of nonlinear stochastic systems, see for instance [33, 35, 41, 42] for an account.

☆Research supported in part by the Brazilian agencies FAPESP Grants 03/06736-7; CNPq Grant 305158/2017-1; 305998/2020-0; 421486/2016-3.

*Corresponding author
Email address: avargas@utfpr.edu.br (Alessandro N. Vargas)

Previous research has shown that when the packet containing information is lost, the system should be reconfigured so as to guarantee stability, a property every system must-have. For instance, the authors of [24] have considered the Bernoulli distribution to model packet dropouts, and the authors of [9] have applied the Bernoulli distribution to handle packet dropouts into in-vehicle networked systems. In another study, the authors of [45] suggest that the feedback signal should remain equal to the last available information, performing a zero-order hold (ZOH). It means the feedback signal is updated only when a new packet reaches the system receiver. Many investigations have supported the idea of using ZOH for handling packet loss under the assumption that the ZOH follows a Markov chain [23, 32, 40, 44]. This paper contributes to this direction, as detailed next.

As for ZOH to handle packet loss, little research has been done on robustness. Existing research has focused on characterizing stochastic stability [45, Thm. 9], but has overlooked robustness. A subsequent study has expanded the result in [45, Thm. 9] to the case of H_∞ control [40, Thm. 1], also with no mention to robustness. In this paper, we expand the usefulness of [40, Thm. 1] and [45, Thm. 9] to the robustness case, as follows.

This paper's main contribution is characterizing the robust stability of stochastic linear systems subject to packet dropouts. We assume the number of samples between successful packet arrivals follows a homogeneous Markov chain, borrowing this assumption from [45]. We then recall a stability result from Markov jump linear systems (e.g., [10], [11]) and use it to characterize the robust second-moment stability of the underlying system.

To clarify the paper's contribution, we now present the system under study. Consider a fixed, filtered probability space $(\Omega, \mathcal{F}, P)$ governing the stochastic linear system

$$x(k+1) = A(\alpha)x(k) + B(\alpha)x(k-\delta(k)) + w(k), \quad \forall k \geq 0, \quad x(0) = x_0 \in \mathbb{R}^n. \tag{1}$$

The process $\{w(k)\}$ represents a vector-valued stochastic process to be defined later. The matrices $A(\alpha)$ and $B(\alpha)$ are not precisely known, but belong to a polytopic domain (e.g., [28, 27]), that is,

$$(A,B)(\alpha) := \left\{ (A,B) : (A,B) = \sum_{j=1}^{\eta} \left(\alpha_j A^{(j)}, \alpha_j B^{(j)} \right) \right\}, \quad \forall \alpha \in \Delta,$$

where Δ is the unit simplex given by

$$\Delta = \left\{ \xi \in \mathbb{R}^\eta : \sum_{i=1}^{\eta} \xi_i = 1,\ \xi_i \geq 0,\ i = 1, \ldots, \eta \right\}$$

and the matrix set $(A^{(1)}, \ldots, A^{(\eta)}, B^{(1)}, \ldots, B^{(\eta)})$ is given. Consider now a sequence of instants $k_0 < k_1 < \cdots < k_i < \cdots$ in (1) such that $k_i \to \infty$ as $i \to \infty$ with probability one. Let these instants denote the index points for which the packets are transmitted successfully—they are called *arrival times*. The interval between two successive arrivals is referred to as *interarrival time*. The next assumption is borrowed from [45].

Assumption 1. ([45]). The interarrival process $\{\theta(i)\}$, defined as $\theta(i) = k_{i+1} - k_i$, $i \geq 0$, follows a homogeneous, finite-dimensional Markov chain.

The process $\{\delta(k)\}$ in (1) represents the delay with resetting at arrival times, that is, $\delta(k)$ equals (see Fig. 1 for a pictorial illustration of $\delta(k)$)

$$\delta(k) = \begin{cases} 0, & \text{if } \ k = k_i, \\ k - k_i, & \text{if } \ k \in (k_i, k_{i+1}). \end{cases}$$

It follows from (1) that, for each $i \geq 0$,

$$x(k+1) = A(\alpha)x(k) + B(\alpha)x(k_i) + w(k), \quad k = k_i, \ldots, k_{i+1} - 1. \tag{2}$$

Remark 1. The stochastic system in (2) retrieves the system studied in [40, 45] when we remove robustness and noise, that is, $(A(\alpha), B(\alpha)) \equiv (A^{(1)}, B^{(1)})$ and $w(k) \equiv 0$. In particular, the authors of [40] have considered a distinct formation rule for $\delta(k)$; namely, $\delta(k)$ can either increase or decrease from k to $k+1$, see [40, Remark 1].

In this paper, we characterize the robust second-moment stability of (2) (see Definition 2.1), i.e., we show that the system (2) is robust second-moment stable if the spectral radius of a certain matrix is less than one (cf., Theorem 2.4). It is difficult to check that spectral radius because the matrix to be evaluated is a function of $(A(\alpha), B(\alpha))$ with a nonlinear dependence of $\alpha \in \Delta$. From the numerical point of view, the condition becomes intractable because infinitely many values of $\alpha \in \Delta$ must be tested.

As an attempt to circumvent this difficulty, we associate Δ with a probability distribution. Instead of taking infinitely many values from Δ, we take only N samples, chosen randomly, and check whether the spectral radius is less than one for their corresponding N matrices. This procedure is called *randomized approach* [7]. A previous study has shown the benefits of the randomized approach for robustness [36]. The randomized approach allows us to show probabilistic bounds for the robust second-moment stability—this procedure turns the problem tractable from the numerical viewpoint. This finding represents the main theoretical contribution of this paper.

This paper also has a contribution to applications. Indeed, an RLC circuit was built in a laboratory to check the usefulness of the randomized approach. The RLC circuit was configured with a closed-loop path subject to packet dropouts—packet dropout means loss of information through the closed-loop path. A microcontroller performed the physical link of the closed-loop path. Besides, the microcontroller was programmed to suffer hardware interruptions according to a Markov chain (see further details in Section 3). These interruptions led to the intermittent transmission of information. The corresponding real-time experiments suggest that the RLC circuit under intermittent closed-loop path be robust second-moment stable, evidence confirmed by the theory of randomized approach. In summary, this paper brings a theoretical novelty and illustrates its potential benefits for applications.

Notation: The symbol $\mathbb{R}^n$ denotes the n-dimensional Euclidean space with its usual norm $\|\cdot\|$. The symbol $\mathbb{R}^{n\times m}$ denotes the space made up by all real-valued matrices of dimension $n \times m$. The spectral radius of a matrix $U \in \mathbb{R}^{n\times n}$ is denoted by $\rho(U)$. The symbol $\otimes$ is used to denote the Kronecker product. The symbol $'$ denotes the transpose of a matrix.

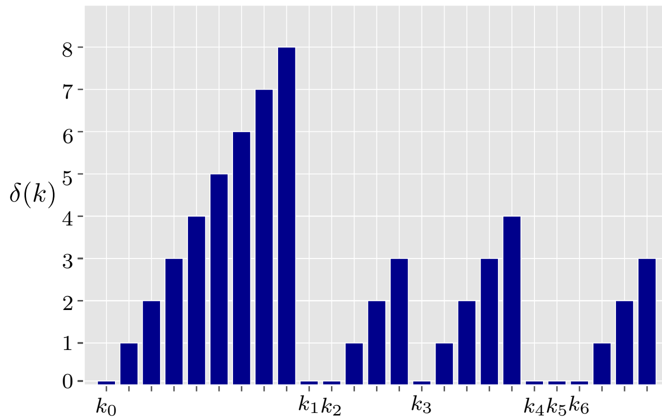

Figure 1: Sample of the delay process $\{\delta(k)\}$: the delay increases linearly. The events $k_0, k_1, \dots$ correspond to the arrival of information with success. When an arrival takes place, the delay resets to zero. The interval between arrivals follows a Markov chain.

2. Definitions and main result

Next we define the stability concept studied in this paper.

Definition 2.1. ([19, Defn. 2.1], [35, Defn. 1]). The stochastic system in (2) is robust second-moment stable if there exists some constant $c = c(x_0)$ such that

$$\mathrm{E}\left[\|x(k)\|^2\right] \leq c, \quad \forall k \geq 0, \quad \forall \alpha \in \Delta.$$

To show the main result of this paper, we consider the next assumption.

Assumption 2. The stochastic process $\{w(k)\}$ is independent and identically distributed, with zero mean and covariance matrix equals $\Sigma = \Sigma' > 0$, that is, $\mathbb{E}[w(k)w(k)'] = \Sigma$ for all $k \geq 0$.

Associated with Assumption 1, the Markov chain $\{\theta(i)\}$ takes values in the finite set $\{1, \dots, N\}$ and evolves according to a given probability matrix, say $P = [p_{\ell j}]$, for all $\ell, j = 1, \dots, N$. The corresponding probability distribution is defined by $\pi_\ell(i) = \Pr(\theta(i) = \ell)$, $\ell = 1, \dots, N$, for each $i \geq 0$.

When a packet arrives successfully at the instant $k = k_i$, the system (2) waits for $\theta(i)$ steps until the arrival of the next packet. This feature into (2) allows us to write

$$x(k_i + n) = \left(A(\alpha)^n + \sum_{m=0}^{n-1} A(\alpha)^m B(\alpha) \right) x(k_i) + \sum_{m=0}^{n-1} A(\alpha)^{n-1-m} w(k_i + m),$$
$$n = 1, \dots, \theta(i). \quad (3)$$

Define

$$M(\alpha, n) = A(\alpha)^n + \sum_{m=0}^{n-1} A(\alpha)^m B(\alpha), \quad \forall n \geq 1.$$

In particular, substituting $k_{i+1} = k_i + n$ and $n = \theta(i)$ into (3) yields

$$x(k_{i+1}) = M(\alpha, \theta(i))x(k_i) + \sum_{m=0}^{\theta(i)-1} A(\alpha)^{\theta(i)-1-m} w(k_i + m). \tag{4}$$

In association with (4), define the second-moment matrix

$$X_\ell(k_i) = \mathrm{E}\left[x(k_i)x'(k_i)\mathbb{1}_{\{\theta(i)=\ell\}}\right] \in \mathbb{R}^{n\times n}, \quad \ell = 1, \ldots, N. \tag{5}$$

This matrix will be useful in characterizing the second-moment stability of (1).

Now we can present the deterministic matrix dynamics that allow us to compute (5).

Lemma 2.2. *For each $i = 0, 1, \ldots$, there holds*

$$X_\ell(k_{i+1}) = \sum_{j=1}^{N} p_{j\ell} M(\alpha, j) X_j(k_i) M(\alpha, j)' + \sum_{j=1}^{N} p_{j\ell}\pi_j(i)\Psi(\alpha, j), \quad \ell = 1, \ldots, N, \tag{6}$$

where

$$\Psi(\alpha, j) = \sum_{m=0}^{j-1} A(\alpha)^{j-1-m}\Sigma(A(\alpha)')^{j-1-m}, \quad j = 1, \ldots, N.$$

Proof. The arguments used in this proof are borrowed from [10, Prop. 3], [11, Prop. 3.35, p. 50] (c.f, [38, Lem. 3.1]). We omit α in all elements shown in the sequence for the sake of notational simplicity. Define

$$\nu(k, n) = \sum_{m=0}^{n-1} A^{n-1-m} w(k + m), \quad \forall n \geq k.$$

It follows from (4) that

$$\begin{aligned}
&\mathrm{E}\left[x(k_{i+1})x(k_{i+1})'\mathbb{1}_{\{\theta(i+1)=\ell\}}\right] \\
&= \sum_{j=1}^{N} \mathrm{E}\left[x(k_{i+1})x(k_{i+1})'\mathbb{1}_{\{\theta(i+1)=\ell,\theta(i)=j\}}\right] \\
&= \sum_{j=1}^{N} \mathrm{E}\big[\big(M(\theta(i))x(k_i) + \nu(k_i, \theta(i))\big)\big(M(\theta(i))x(k_i) + \nu(k_i, \theta(i))\big)'\mathbb{1}_{\{\theta(i+1)=\ell,\theta(i)=j\}}\big].
\end{aligned}$$

Considering in the above expression the fact that $x(k)$ and $w(k)$ are independent random variables (i.e., $\mathbb{E}[x(k)w(k)'] = \mathbb{E}[x(k)]\mathbb{E}[w(k)']$) and $\mathbb{E}[w(k)] = 0$ (see Assumption 2), we obtain

$$\begin{aligned}
&\mathrm{E}\left[x(k_{i+1})x(k_{i+1})'\mathbb{1}_{\{\theta(i+1)=\ell\}}\right] \\
&= \sum_{j=1}^{N} \mathrm{E}\left[\big(M(\theta(i))x(k_i)x(k_i)'M(\theta(i))' + \nu(k_i, \theta(i))\nu(k_i, \theta(i))'\big)\mathbb{1}_{\{\theta(i+1)=\ell,\theta(i)=j\}}\right].
\end{aligned} \tag{7}$$

Recall that

$$\Pr(\theta(i+1)=\ell, \theta(i)=j) = \Pr(\theta(i)=j)p_{j\ell} = \mathrm{E}[\mathbb{1}_{\{\theta(i)=j\}}]p_{j\ell}.$$

As a result, the right-hand side of (7) equals

$$\sum_{j=1}^{N} p_{j\ell} M(j)\mathrm{E}[x(k_i)x(k_i)'\mathbb{1}_{\{\theta(i)=j\}}]M(j)' + \sum_{j=1}^{N} p_{j\ell}\Pr(\theta(i)=j)\mathrm{E}[\nu(k_i,j)\nu(k_i,j)']. \tag{8}$$

Now we evaluate the rightmost term of (8). Since $\mathrm{E}[w(k)w(k)'] = \Sigma$ for all $k \geq 0$, and $\mathrm{E}[w(k)w(m)'] = 0$ when $k \neq m$, we obtain

$$\begin{aligned} \mathrm{E}[\nu(k_i,j)\nu(k_i,j)'] &= \mathrm{E}\left[\left(\sum_{m=0}^{j-1} A^{j-1-m}w(k_i+m)\right)\left(\sum_{m=0}^{j-1} A^{j-1-m}w(k_i+m)\right)'\right] \\ &= \sum_{m=0}^{j-1} A^{j-1-m}\Sigma(A')^{j-1-m}. \end{aligned} \tag{9}$$

Substituting (9) into (8) yields the result. □

Remark 2. What Lemma 2.2 reveals is that the dynamical behavior of (2) is equivalent to the dynamical behavior of the following Markov jump linear system,

$$y(i+1) = M(\alpha,\theta(i))y(i) + \Psi(\alpha,\theta(i))^{\frac{1}{2}}w(i), \quad \forall i \geq 0, \quad y(0) = x_0 \in \mathbb{R}^n. \tag{10}$$

Indeed, by setting $Y_\ell(i) = \mathrm{E}\left[y(i)y'(i)\mathbb{1}_{\{\theta(i)=\ell\}}\right] \in \mathbb{R}^{n\times n}$, $\ell = 1,\dots,N$, the authors of [10, Prop. 3] (see [11, Prop. 3.35, p. 50]) show that $Y_\ell(i)$ satisfies (6) with $X_\ell(k_i) = Y_\ell(i)$, for each $i \geq 0$. As a result, the stability of (2) is equivalent to the stability of the Markov jump linear system in (10). This fact is summarized in the following result.

Proposition 2.3. *The system in* (2) *is second-moment stable if and only if the Markov jump linear system in* (10) *is second-moment stable.*

Now we recall the result from the literature that allows us to characterize the second-moment stability of (10) (e.g., [10], [11, Ch. 3, p. 34]). Define the matrix $\mathcal{A}(\alpha) \in \mathbb{R}^{Nn^2\times Nn^2}$ as

$$\mathcal{A}(\alpha) = (P' \otimes I_{n^2})\begin{bmatrix} M(\alpha,1)\otimes M(\alpha,1) & & \\ & \ddots & \\ & & M(\alpha,N)\otimes M(\alpha,N)\end{bmatrix}. \tag{11}$$

Applying the stacking vector operator $\mathrm{vec}(\cdot)$ on both sides of (6) (with $X_\ell(k_i) = Y_\ell(i)$), we obtain (see [10], [11, Ch. 3])

$$z(i+1) = \mathcal{A}(\alpha)z(i) + \varphi(\alpha,i), \quad z(0) \in \mathbb{R}^{Nn^2}, \tag{12}$$

where $\varphi(\alpha, i) \in \mathbb{R}^{Nn^2}$ depends only on some arrangements upon $\pi(i)$, $\mathbb{P}$, and $\Psi(\alpha, i)$. The system state $z(i) \in \mathbb{R}^{Nn^2}$ equals

$$z(i) = \begin{bmatrix} \operatorname{vec}(Y_1(i)) \\ \vdots \\ \operatorname{vec}(Y_N(i)) \end{bmatrix}, \quad \forall i \geq 0.$$

Suppose for the moment that $\sup_{\alpha\in\Delta} \rho(\mathcal{A}(\alpha)) < 1$. Then there exists some constant $c > 0$ (which may depend on $z(0)$) such that $\|z(i)\|^2 \leq c$, for all $i \geq 0$ (e.g., [21, Thm. 2]). The next result then follows from Proposition 2.3 because of the equivalence between (10) and (12).

Theorem 2.4. *Let the matrix $\mathcal{A}(\alpha) \in \mathbb{R}^{Nn^2\times Nn^2}$ be as in* (11)*. Then the system* (2) *is robust second-moment stable if and only if*

$$\sup_{\alpha\in\Delta} \rho(\mathcal{A}(\alpha)) < 1. \tag{13}$$

Remark 3. The result in Theorem 2.4 works under the assumption that the covariance-noise matrix Σ is positive definite (see Assumption 2). If Σ is not positive, then the robust second-moment stability of (2) may not imply in (13).

Remark 4. When the system (2) is not affected by uncertain parameters (i.e, $(A(\alpha), B(\alpha)) \equiv (A^{(1)}, B^{(1)})$) and no noise (i.e., $w(k) \equiv 0$), Theorem 2.4 reduces to the result in [40, Thm. 1] and [45, Thm. 9]. For this reason, Theorem 2.4 can be interpreted as an extension of the result in [40, Thm. 1] and [45, Thm. 9].

Remark 5. Theorem 2.4 requires computing the spectral-radius of the polynomial matrix $\mathcal{A}(\alpha)$ (degree N) for all $\alpha \in \Delta$. To the best of the authors' knowledge, there is no method to compute that spectral-radius for all $\alpha \in \Delta$, because $\mathcal{A}(\alpha)$ is a nonlinear function with respect to $\alpha \in \Delta$. As an attempt to overcome this problem, one could perform such computation through robust stability analysis conditions for uncertain systems based on linear matrix inequality relaxations [9, Ch. 4], [28]. Yet, the computational burden rapidly becomes prohibitive, even for small dimension systems. Moreover, such procedures are in general only semi-decidable, not allowing to certificate infeasibility. This numerical difficulty motivated us to convert the problem of checking the stability of (13) into a probabilistic problem, as detailed next.

2.1. Randomized approach for checking robust stability

To check the robust stability of the system (2), we deploy the randomized approach [7]. The idea is to convert the simplex Δ into a random variable, as suggested in [4, 5, 36].

Assumption 3. ([4, p. 29], [36]). The simplex Δ is endowed with a probability measure $\mathbb{P}$ over all the subsets of the underlying σ-algebra.

The randomized evaluation for checking the robust stability of (2) is as follows. Under the measure $\mathbb{P}$, take some constant $\beta > 0$ and define (e.g., [5])

$$p(\beta) = \mathbb{P}\left[\rho(\mathcal{A}(\alpha)) < \beta\right]. \tag{14}$$

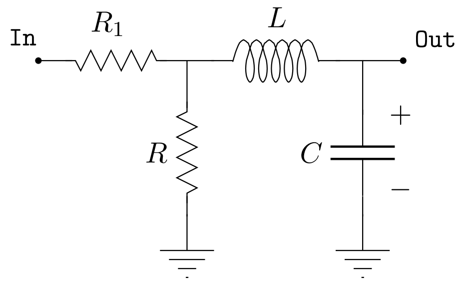

Figure 2: RLC circuit.

The constant $\beta > 0$ in (14) acts like a stability margin, a term coined by the authors of [5]. Now, using the probability distribution associated with $\mathbb{P}$, we take n samples from Δ, chosen randomly and independently from each other, say $\alpha^{(1)}, \ldots, \alpha^{(n)}$. We want to evaluate how many elements from that sample respect the condition $\rho(\mathcal{A}(\alpha^{(i)})) < \beta$. To do so, we compute the empirical probability

$$\hat{p}_n(\beta) = \frac{1}{n} \sum_{i=0}^{n} \mathbb{1}_{\{\rho(\mathcal{A}(\alpha^{(i)}))<\beta\}}. \tag{15}$$

Recall that the law of large numbers assures that $\hat{p}_n(\beta)$ tends to $p(\beta)$ when n tends to infinity. Even though this result allows us to approximate the value of $p(\beta)$ under arbitrarily small precision, it would require us to sample the simplex Δ infinitely many times—a prohibitive approach. To overcome this numerical restriction, we can deploy the Hoeffding's inequality to obtain the next result [18], which follows as a particular case of the Chernoff bound [5].

Proposition 2.5. *For each sufficiently small $\varepsilon > 0$, there holds*

$$\Pr\left[|p(\beta) - \hat{p}_n(\beta)| \geq \varepsilon\right] \;\leq\; 2\exp(-2\varepsilon^2 n).$$

Proposition 2.5 is effective in giving us a probability measure for the robust stability of the system (2). For instance, suppose we use (15) to compute $\hat{p}_{n_0}(0.9)$ for $n_0 = 2 \times 10^7$ samples taken randomly from Δ. Assume that the evaluation yields $\hat{p}_{n_0}(0.9) = 1$. Proposition 2.5 then assures that the probability of $p(0.9)$ lying within the interval $[0.9995, 1]$ is at least $1 - 2\exp(-2 \times 0.0005^2 \times n_0) = 0.99995$. Being close to one, this value means that the inequality

$$\sup_{\alpha\in\Delta} \rho(\mathcal{A}(\alpha)) < 0.9 \tag{16}$$

is likely to be true under a high probability. However, care should be exercised when using this randomized approach in sensitive applications because randomization cannot guarantee that (16) holds with probability one (see [6, 7] for further details).

3. Experiments for RLC circuit

The experiments described in this section were derived to illustrate the potential of Theorem 2.4, together with Proposition 2.5, for applications.

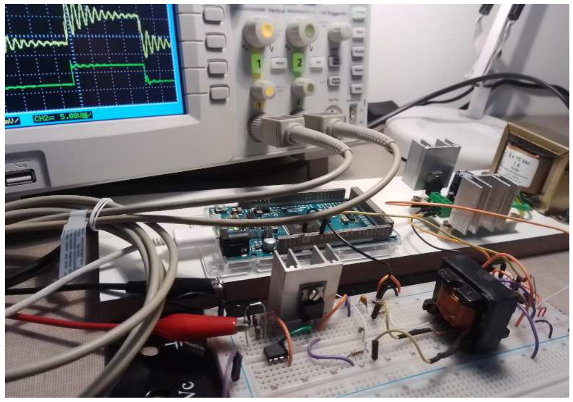

Figure 3: Experimental setup. The RLC circuit was built in the breadboard. An oscillating signal from the circuit output is shown in the oscilloscope screen.

The experimental setup considers a circuit containing resistor (R), inductor (L), and capacitor (C), known as RLC circuit (Fig. 2). RLC circuits are ubiquitous in the electronics industry [12], finding applications in a broad spectrum of fields, such as flexible electronics [20], smart screen [29], electromagnetic device [49], temperature sensor [3], antenna [2], bacteria sterilization [17], and brain stimulator [39]. RLC circuits are particularly useful in applications that depend upon oscillating signals [22, 30, 31]. Many of these circuits work in a modified design that includes a closed-loop path, a strategy used to minimize the effects of disturbances that could distort the shape of the oscillating signal [15, 31]. This paper presents a contribution towards understanding the effects of the closed-loop path in distorting oscillating signals, as detailed next.

Oscillating signals were generated in a laboratory (Fig. 3). The RLC circuit components were chosen to let the circuit produce an underdamped, oscillatory response when the circuit input received voltage steps. Afterwards the circuit was modified to include a closed-loop path.

The motivation behind the experiment was to assess how distorted an oscillating signal becomes when interruption takes place in the closed-loop path. By interruption, we mean the event that suspends the flow of information through the closed-loop. Interruption is a common phenomenon in microcontrollers [14, Ch. 7]; recall that they have internal processors that temporarily interrupt their main routines to process other tasks, taking a certain amount of time in the interrupted mode. While the microcontroller keeps processing other tasks, the main routine remains stopped. As a result, the microcontroller's main routine works under an intermittent processing. When random events drive the interruptions, the intermittent processing becomes random as well. Random events are common for those real-time applications.

We wanted to check how random, intermittent processing affects the RLC circuit. A microcontroller, programmed to show intermittent processing, was included in the circuit's closed-loop path. As we shall see, the intermittent processing led to distortion on the oscillating signal, yet the result of Theorem 2.4 guarantees the circuit's robust stability. More details about the experiments are given in the sequence.

3.1. Modeling and identification of the RLC circuit

Let $x(t) \in \mathbb{R}^2$, $\forall t \geq 0$, be the continuous-time representation of the RLC circuit (see Fig. 2), where $x_{[1]}(t)$ and $x_{[2]}(t)$ denote the current in the inductor L and the voltage in the capacitor C, respectively. Let $u(t) \in \mathbb{R}$ be the circuit input (Volts) and let $y(t) = x_{[2]}(t) \in \mathbb{R}$ be the circuit output (Volts). A circuit analysis allows us to model the RLC circuit as (e.g., [13, 37])

$$\frac{\mathrm{d}x(t)}{\mathrm{d}t} = \begin{bmatrix} -\frac{R_1 R}{L(R_1+R)} & -\frac{1}{L} \\ \frac{1}{C} & 0 \end{bmatrix} x(t) + \begin{bmatrix} \frac{R}{L(R_1+R)} \\ 0 \end{bmatrix} u(t), \quad \forall t \geq 0. \tag{17}$$

For identification, we applied voltage steps in $u(t)$ and compared the experimental data with the simulation data, see Fig. 4. In the simulation, we assumed that the capacitor and resistors had the values informed by their manufacturers, which are $C = 0.1\,\mu\mathrm{F}$, $R_1 = 10\,\Omega$, and $R = 150\,\Omega$. The inductor was constructed manually, and its inductance was measured and had a value of $L = 1.54\,\mathrm{mH}$.

According to their manufacturers, the resistors and capacitors comply with $\pm 5\%$ tolerance. It means that the exact values of R_1, R, and C are uncertain. Consequently, we can interpret the system (17) as an uncertain system. In addition, these component values are bounded, which means that we can convert the uncertain system into a polytopic system. To advance our analysis, we convert that polytopic version of (17) directly into its discrete-time counterpart, as follows. We combine the extreme values of the components with the zero-order hold in (17) to obtain (with sampling time fixed at 1.5 microseconds)

$$x(k+1) \;=\; \underbrace{\begin{bmatrix} a_{11}(\alpha) & a_{12}(\alpha) \\ a_{21}(\alpha) & a_{22}(\alpha) \end{bmatrix}}_{A(\alpha)} x(k) + \underbrace{\begin{bmatrix} b_1(\alpha) \\ b_2(\alpha) \end{bmatrix}}_{B(\alpha)} u(k), \quad \forall k \geq 0, \quad \forall \alpha \in \Delta, \tag{18}$$

where the vertices $a_{11}^{(n)}, \dots, a_{22}^{(n)}, b_1^{(n)}, b_2^{(n)}$, $n = 1, \dots, 8$, are given in Table 1. The system output is

$$y(k) \;=\; [0 \;\; 1] x(k), \quad \forall k \geq 0.$$

3.2. RLC circuit with intermittent closed-loop path

The RLC circuit with an intermittent closed-loop path was built in laboratory, see Fig. 5. As can be seen, the RLC circuit received the command input $u(k)$ from the driver (for the sake of completeness, we present the driver's schematic in Fig. 8, Appendix). The driver was fed by the signal $e(k)$, and oscilloscope measurements indicated that $u(k) = 3e(k) + 2.6$ (Volts), see Appendix. The signal $e(k)$ was generated by an analog differential amplifier. This amplifier was built with an op-amp LM358 and had the unique purpose of subtracting the signal generated by the microcontroller from the signal $r(k)$ generated by a voltage-step source. The microcontroller used in the experiments was an Arduino Due (with sampling time programmed to be 1.5 milliseconds).

Remark 6. The only task of the Arduino Due was to implement the on-off switch (see Fig. 5). This switch opened and closed the feedback path in a random way. That is, the amount

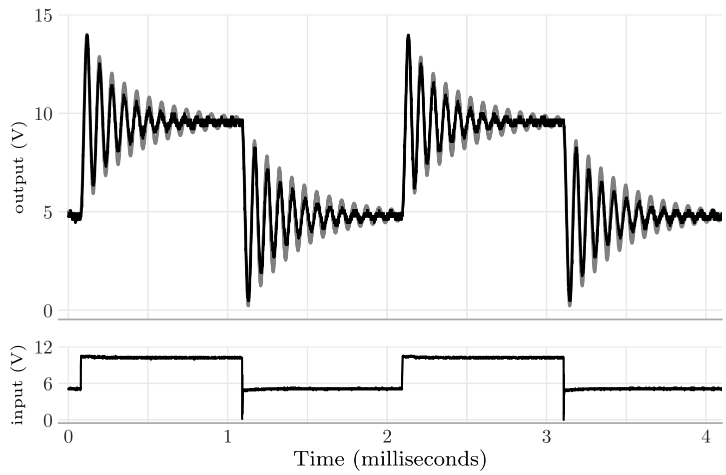

Figure 4: Data used in the identification of the RLC circuit. The simulation data (gray) approximate the experimental data (black).

of time for which the switch remained either on or off was programmed to follow a Markov chain, as follows. Recall that the interarrival process $\{\theta(i)\}$ (with $\theta(i) = k_{i+1} - k_i$) follows a Markov chain with probability transition $\mathbb{P}$. The arrival times $k_0 < k_1 < \cdots < k_i < \cdots$ were generated into the Arduino Due by an algorithm that took random samples based on $\mathbb{P}$ (to be defined in the sequence). As a result, the Arduino Due generated the samples of the arrival times $\delta(k)$, which equals (see Fig. 1)

$$\delta(k) = \begin{cases} 0, & \text{if } \ k = k_i, \\ k - k_i, & \text{if } \ k \in (k_i, k_{i+1}). \end{cases}$$

When the switch was 'on', the output became available instantaneously to the driver. But when the switch was 'off', the microcontroller transmitted the last output available. In formal terms, the signal $e(k)$ equals

$$e(k) = \begin{cases} r(k) - y(k), & \text{if } k = k_i, \\ r(k) - y(k_i), & \text{if } k_i < k < k_{i+1}, \end{cases}$$

where k_i represents the i-th occasion in which the switch visited the 'on' mode and $r(k)$ denotes a reference signal. The switch was programmed to follow a homogeneous Markov chain with probability matrix defined as

$$\mathbb{P} = \begin{bmatrix} \mathbf{0}_{\mathbf{30}\times\mathbf{90}} & I_{30} \\ \mathbf{0}_{\mathbf{90}\times\mathbf{30}} & \frac{1}{90}U_{90} \end{bmatrix} \in \mathbb{R}^{120\times 120}$$

where $I_{30} \in \mathbb{R}^{30\times 30}$ represents the identity matrix and $U_{90} \in \mathbb{R}^{90\times 90}$ represents the matrix containing all of its entries equal to one.

Finally, we can combine the definitions mentioned above, together with (18), to attain the model representing the RLC circuit with intermittent closed-loop path. It reads as

$$x(k+1) = A(\alpha)x(k) + B(\alpha)Cx(k - \delta(k)) + d(\alpha, k), \quad \forall k \geq 0, \quad \alpha \in \Delta, \tag{19}$$

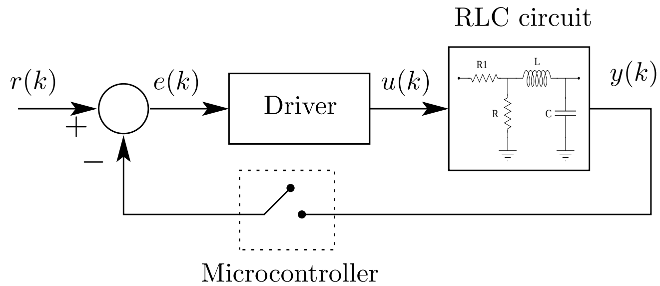

Figure 5: RLC circuit under intermittent closed-loop path. The driver amplifies the signal $e(k)$ and feeds the RLC circuit through $u(k)$. The microcontroller acts as an on-off switch. The amount of time for which the switch remains either on or off depends on a Markov chain.

where $C = [0 \quad -3]$, and the rightmost term of (19) equals

$$d(\alpha, k) := B(\alpha)(3r(k) + 2.6) + w(k).$$

The Gaussian noise $w(k) \in \mathbb{R}^2$ was included to account for real-time noise observed in the measurements.

3.3. Statistical analysis

Define the robust matrix $\mathcal{A}(\alpha)$ as in (11) with parameters as in (19). Now, we can claim that the inequality

$$\sup_{\alpha \in \Delta} \rho(\mathcal{A}(\alpha)) < 0.95 \tag{20}$$

is likely to be true under a high probability. Indeed, we took $n_0 = 7.5 \times 10^5$ samples from Δ, uniformly distributed, and obtained $\hat{p}_{n_0}(0.95) = 1$ from (15). It then follows from Proposition 2.5 that the probability

$$p(0.95) = \mathbb{P}\left[\rho(\mathcal{A}(\alpha)) < 0.95\right]$$

lies within the interval $[0.998, 1]$ with chance of occurrence of more than $1 - 2\exp(-2 \times 0.002^2 \times n_0) = 0.995$. This statistical outcome suggests that the inequality in (20) is likely to be true, which implies that the system (19) is likely to be robust second-moment stable under a high probability.

3.4. Experiments for the RLC circuit in closed-loop

The reference signal $r(k)$ in Fig. 5 is a square wave oscillating between 0V and 3.8V. The step-up from 0V to 3.8V and the step down from 3.8V to 0V form what we call *pulse step*. Pulse steps were adjusted to occur at the 500Hz frequency.

Experiments were then carried out in the laboratory, and a sample is depicted in Fig. 6. The experimental data indicate that the oscillating signal from the RLC circuit became distorted due to the intermittent closed-loop path.

We became interested in checking the role of distortion upon the circuit through more experiments. Two-hundred pulse steps were then applied in the circuit. The experimental data indicate that the circuit was stable, even though distortion persists, see Fig. 7. This

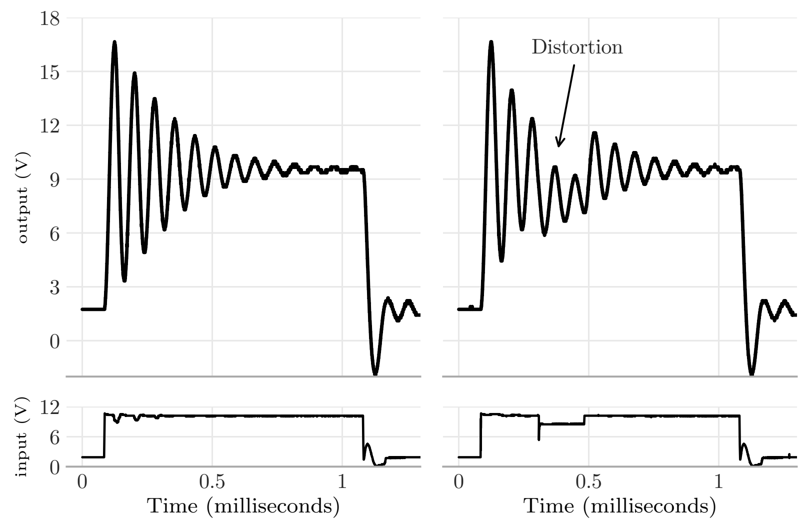

Figure 6: Experimental data from the RLC circuit with a closed-loop path. Curves on the left side represent the closed-loop path working continuously (the switch remained 'on' all the time). Curves on the right represent the case under an intermittent closed-loop path. The distortion appears in this case, as indicated in the picture.

experimental evidence confirms the result of Theorem 2.4 and Proposition 2.5, as statistical data suggested that the circuit be robust second-moment stable under a high probability (see Section 3.3).

In summary, the experiments of this section confirm the usefulness of Theorem 2.4, together with Proposition 2.5, for real-time applications.

4. Concluding remarks

This paper has shown a spectral-radius condition that characterizes the robust second-moment stability of linear stochastic systems subject to packet loss. The idea is that packets are lost due to transmission failures. We have assumed that the packets-loss process follows a Markov chain, as suggested in [45]. We then show that our approach

n	$a_{11}^{(n)}$	$a_{12}^{(n)}$ $[\times 10^{-4}]$	$a_{21}^{(n)}$	$a_{22}^{(n)}$	$b_1^{(n)}$ $[\times 10^{-4}]$	$b_2^{(n)}$ $[\times 10^{-3}]$
1	0.9835	-9.6712	14.18	0.9930	9.0668	6.4941
2	0.9828	-9.6688	15.67	0.9923	9.0645	7.1770
3	0.9836	-9.6715	14.18	0.9930	9.0078	6.4518
4	0.9828	-9.6691	15.67	0.9923	9.0050	7.1301
5	0.9844	-9.6754	14.19	0.9930	9.1250	6.5349
6	0.9836	-9.6730	15.68	0.9923	9.1227	7.2219
7	0.9844	-9.6756	14.19	0.9930	9.0709	6.4961
8	0.9837	-9.6732	15.68	0.9923	9.0687	7.1790

Table 1: Entries of the vertices of the uncertain, discrete-time system (18).

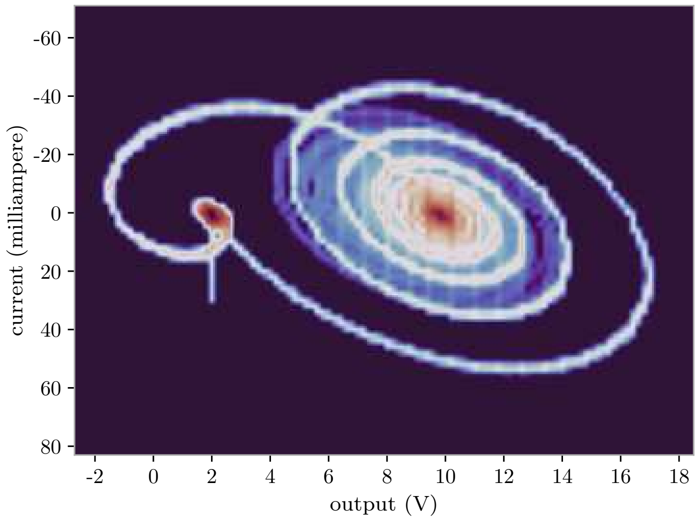

Figure 7: Phase portrait of the current in the inductor versus the voltage in the capacitor: data from two-hundred pulse steps. The trajectories move in the anticlockwise direction. The light-blue area spreading around the right eye indicates the distortion, a phenomenon that deviated many trajectories from the oscillating path (white curve). All trajectories remained stable, evidence that confirms the result of Theorem 2.4.

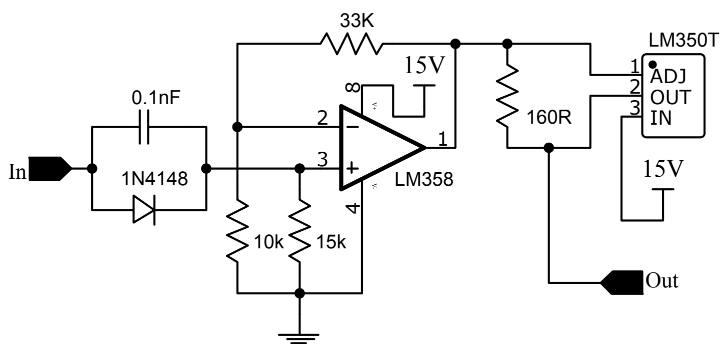

Figure 8: (Appendix). Schematic for the electronic driver. It was used in the laboratory described in Section 3.

expands the results in [40, Thm. 1] and in [45, Thm. 9] to cope with robustness (see Remark 5 in connection).

A drawback of the robust approach is that it requires evaluating the spectral radius of a matrix that depends on both $A(\alpha)$ and $B(\alpha)$, for all $\alpha \in \Delta$, specially for high-dimensional systems. To the best of the authors' knowledge, there is no efficient tool to do that evaluation. For this reason, and motivated by the paper's RLC circuit application, we have decided to convert the robustness problem into a probabilistic problem, called randomized approach [7]. As for the randomized approach, we select N samples from Δ and calculate their corresponding statistics. The statistics allow us to calculate the probability in which the spectral radius satisfies the desired condition. In other words, we have developed a strategy that assures the system is robust second-moment stable under high probability. However, more research into robust stability is still necessary because our probabilistic approach does not give a definitive (i.e., deterministic) answer to the stability problem.

We have seen that the paper's finding is useful for applications. The paper shows laboratory experiments that included an RLC circuit under a closed loop. The aim was to check how oscillating signals become distorted under an intermittent closed-loop path. A packet-loss process was introduced in the closed-loop to produce that intermittent behavior. Experimental data confirmed that the RLC circuit was stable even under distortion, evidence that agrees with the theoretical findings.

Appendix

The driver schematics of Fig. 8 was mounted in a laboratory. The driver was used in the control scheme shown in Fig. 5. Analyzing the circuit of Fig. 8, we can conclude that the voltage input and output, say V_{in} and V_{out}, follow the next relation:

$$V_{out} = \begin{cases} c + 4.3V_{in}, & \text{if } V_{in} > 0, \\ 0, & \text{otherwise,} \end{cases}$$

where $c > 0$ is some constant that depends on both the voltage across the diode 1N4148 and the internal voltage reference of the regulator LM350T. Oscilloscope measurements made in the laboratory indicated that $V_{out} = 2.6 + 3V_{in}$. Notice that the constant multiplying V_{in} differs from that of the circuit analysis, possibly due to a mismatch of values in components. This experimental finding allowed us to conclude that driver shown in Fig. 5 can be represented as $u(k) = 2.6 + 3e(k)$ because $e(k) = V_{in}$ was positive for all experiments.

References

[1] Aatabe, M., Guezar, F.E., Bouzahir, H., Vargas, A.N., 2020. Constrained stochastic control of positive Takagi-Sugeno fuzzy systems with Markov jumps and its application to a DC-DC boost converter. Transactions of the Institute of Measurement and Control 42, 3234–3242.

[2] Adams, J.J., Bernhard, J.T., 2013. Broadband equivalent circuit models for antenna impedances and fields using characteristic modes. IEEE Transactions on Antennas and Propagation 61, 3985–3994.

[3] Albrecht, A., Salmeron, J.F., Becherer, M., Lugli, P., Rivadeneyra, A., 2019. Screen-printed chipless wireless temperature sensor. IEEE Sensors Journal 19, 12011–12015.

[4] Calafiore, G., Campi, M.C., 2005. Uncertain convex programs: randomized solutions and confidence levels. Mathematical Programming 102, 25–46.

[5] Calafiore, G.C., Dabbene, F., Tempo, R., 2000. Randomized algorithms for probabilistic robustness with real and complex structured uncertainty. IEEE Transactions on Automatic Control 45, 2218–2235.

[6] Calafiore, G.C., Dabbene, F., Tempo, R., 2011. Research on probabilistic methods for control system design. Automatica 47, 1279–1293.

[7] Campi, M.C., 2010. Why is resorting to fate wise? A critical look at randomized algorithms in systems and control. European Journal of Control 16, 419 – 430.

[8] Casado-Vara, R., Novais, P., Gil, A.B., Prieto, J., Corchado, J.M., 2019. Distributed continuous-time fault estimation control for multiple devices in IoT networks. IEEE Access 7, 11972–11984.

[9] Chang, X.H., Liu, Y., 2020. Robust H_∞ filtering for vehicle sideslip angle with quantization and data dropouts. IEEE Transactions on Vehicular Technology 69, 10435–10445.

[10] Costa, O.L.V., Fragoso, M.D., 1993. Stability results for discrete-time linear systems with Markovian jumping parameters. J. Math. Anal. Appl. 179, 154–178.

[11] Costa, O.L.V., Fragoso, M.D., Marques, R.P., 2005. Discrete-Time Markovian Jump Linear Systems. Springer-Verlag, New York.

[12] Darlington, S., 1999. A history of network synthesis and filter theory for circuits composed of resistors, inductors, and capacitors. IEEE Transactions on Circuits and Systems I: Fundamental Theory and Applications 46, 4–13.

[13] Faleski, M.C., 2006. Transient behavior of the driven RLC circuit. American Journal of Physics 74, 429–437.

[14] Gimenez, S.P., 2018. 8051 Microcontrollers: Fundamental Concepts, Hardware, Software and Applications in Electronics. Springer, New York, NY.

[15] Gokcek, C., 2003. Tracking the resonance frequency of a series RLC circuit using a phase locked loop, in: Proc. 2003 IEEE Conf. Control Applications, 2003. CCA 2003., pp. 609–613.

[16] Haghighi, P., Tavassoli, B., Farhadi, A., 2020. A practical approach to networked control design for robust H_∞ performance in the presence of uncertainties in both communication and system. Applied Mathematics and Computation 381, 125308.

[17] Hee-Kyu Lee, Suehiro, J., Hara, M., Duck-Chul Lee, Myung-Hwan So, 2000. Energy efficiency improvement of electrical sterilization using oscillatory waveforms from a RLC discharging circuit. IEEE Transactions on Dielectrics and Electrical Insulation 7, 872–874.

[18] Hoeffding, W., 1963. Probability inequalities for sums of bounded random variables. Journal of the American Statistical Association 58, 13–30.

[19] Huang, L., Mao, X., 2009. On input-to-state stability of stochastic retarded systems with Markovian switching. IEEE Transactions on Automatic Control 54, 1898–1902.

[20] Khan, Y., Thielens, A., Muin, S., Ting, J., Baumbauer, C., Arias, A.C., 2020. A new frontier of printed electronics: Flexible hybrid electronics. Advanced Materials 32, 1905279.

[21] Kubrusly, C.S., 1988. Uniform stability for time-varying infinite-dimensional discrete linear systems. IMA J. Math. Control Inform. 5, 269–283.

[22] Lee, T.H., Hajimiri, A., 2000. Oscillator phase noise: a tutorial. IEEE Journal of Solid-State Circuits 35, 326–336.

[23] Li, H., Chow, M., Sun, Z., 2009. Optimal stabilizing gain selection for networked control systems with time delays and packet losses. IEEE Transactions on Control Systems Technology 17, 1154–1162.

[24] Li, Z.M., Chang, X.H., Yu, L., 2016. Robust quantized H_∞ filtering for discrete-time uncertain systems with packet dropouts. Applied Mathematics and Computation 275, 361–371.

[25] Mohammadzadeh, A., Tavassoli, B., Moaveni, B., 2020. Simultaneous estimation of state and packet-loss occurrences in networked control systems. ISA Transactions 107, 307–315.

[26] Nguyen, V., Kim, O.T.T., Pham, C., Oo, T.Z., Tran, N.H., Hong, C.S., Huh, E., 2018. A survey on adaptive multi-channel MAC protocols in VANETs using Markov models. IEEE Access 6, 16493–16514.

[27] Oliveira, R.C.L.F., Peres, P.L.D., 2007. Parameter-dependent LMIs in robust analysis: Characterization of homogeneous polynomially parameter-dependent solutions via LMI relaxations. IEEE Transactions on Automatic Control 52, 1334–1340.

[28] Oliveira, R.C.L.F., Peres, P.L.D., 2008. A convex optimization procedure to compute H_2 and H_∞ norms for uncertain linear systems in polytopic domains. Optimal Control Applications and Methods 29, 295–312.

[29] Pereira, N., Correia, V., Peřinka, N., Costa, C.M., Lanceros-Méndez, S., 2021. All-printed smart label with integrated humidity sensors and power supply. Advanced Engineering Materials 23, 2001229. doi:10.1002/adem.202001229.

[30] Quiroz-Juárez, M., Jiménez-Ramírez, O., Aragón, J., Del Río-Correa, J., Vázquez-Medina, R., 2019. Periodically kicked network of RLC oscillators to produce ECG signals. Computers in Biology and Medicine 104, 87–96.

[31] Senani, R., Bhaskar, D.R., Singh, V.K., Sharma, R.K., 2016. Sinusoidal oscillators and waveform generators using modern electronic circuit building blocks. volume 622. Springer, New York, NY.

[32] Shen, D., Xu, J., 2017. A novel Markov chain based ILC analysis for linear stochastic systems under general data dropouts environments. IEEE Transactions on Automatic Control 62, 5850–5857.

[33] Shen, H., Li, F., Xu, S., Sreeram, V., 2018. Slow state variables feedback stabilization for semi-Markov jump systems with singular perturbations. IEEE Transactions on Automatic Control 63, 2709–2714.

[34] Shi, Y., Huang, J., Yu, B., 2013. Robust tracking control of networked control systems: Application to a networked DC motor. IEEE Transactions on Industrial Electronics 60, 5864–5874.

[35] Vargas, A.N., Filho, S.M., Agulhari, C.M., Montezuma, M.A.F., Costa, E.F., 2020. Stabilizing nonlinear Markov jump systems with orthogonality between control and nonlinear terms. International Journal of Robust and Nonlinear Control 30, 5122–5133.

[36] Vargas, A.N., Montezuma, M.A., Liu, X., Oliveira, R.C., 2019. Robust stability of Markov jump linear systems through randomized evaluations. Applied Mathematics and Computation 346, 287–294.

[37] Vargas, A.N., Pujol, G., Acho, L., 2017. Stability of Markov jump systems with quadratic terms and its application to RLC circuits. Journal of the Franklin Institute 354, 332–344.

[38] Vargas, A.N., do Val, J.B.R., Costa, E.F., 2004. Receding horizon control of Markov jump linear systems subject to noise and unobservable state chain, in: Proc. 43th IEEE Conf. Decision Control, pp. 4381–4386.

[39] Wagner, T., Valero-Cabre, A., Pascual-Leone, A., 2007. Noninvasive human brain stimulation. Annual Review of Biomedical Engineering 9, 527–565.

[40] Wang, D., Wang, J., Wang, W., 2013. H_∞ controller design of networked control systems with Markov packet dropouts. IEEE Transactions on Systems, Man, and Cybernetics: Systems 43, 689–697.

[41] Wang, J., Xia, J., Shen, H., Xing, M., Park, J.H., 2020a. H_∞ synchronization for fuzzy Markov jump chaotic systems with piecewise-constant transition probabilities subject to PDT switching rule. IEEE Transactions on Fuzzy Systems , 1–1doi:10.1109/TFUZZ.2020.3012761.

[42] Wang, J., Yang, C., Shen, H., Cao, J., Rutkowski, L., 2020b. Sliding-mode control for slow-sampling singularly perturbed systems subject to Markov jump parameters. IEEE Transactions on Systems, Man, and Cybernetics: Systems , 1–8doi:10.1109/TSMC.2020.2979860.

[43] Wen, S., Guo, G., 2019. Observer-based control of vehicle platoons with random network access. Robotics and Autonomous Systems 115, 28–39.

[44] Xia, Y., Xie, W., Zhu, Z., Wang, G., Wang, X., 2013. Performance analysis of networked predictive control systems with data dropout. Optimal Control Applications and Methods 34, 742–756.

[45] Xiong, J., Lam, J., 2007. Stabilization of linear systems over networks with bounded packet loss. Automatica 43, 80–87.

[46] Xu, Y., Yang, L., Wang, Z., Rao, H., Lu, R., 2020. State estimation for networked systems with Markov driven transmission and buffer constraint. IEEE Transactions on Systems, Man, and Cybernetics: Systems , 1–8doi:10.1109/TSMC.2020.2980425.

[47] Yang, H., Xu, Y., Zhang, J., 2017. Event-driven control for networked control systems with quantization and Markov packet losses. IEEE Transactions on Cybernetics 47, 2235–2243.

[48] Zhang, X., Han, Q., Yu, X., 2016. Survey on recent advances in networked control systems. IEEE Transactions on Industrial Informatics 12, 1740–1752.

[49] Zhang, X., Zhang, X., Fu, W.N., 2017. Fast numerical method for computing resonant characteristics of electromagnetic devices based on finite-element method. IEEE Transactions on Magnetics 53, 1–4.